Tetragonal distortion of Mn films on $Cu_3Au(100)$

B. Schirmer, B. Feldmann, and A. Sokoll
Institut für Grenzflächenforschung und Vakuumphysik, Forschungszentrum Jülich, 52428 Jülich, Germany

Y. Gauthier
Laboratoire de Crystallographie, CNRS, Boite Postale 166 X, 38042 Grenoble, France

M. Wuttig
Institut für Grenzflächenforschung und Vakuumphysik, Forschungszentrum Jülich, 52428 Jülich, Germany and I. Physikalisches Institut der RWTH Aachen, 52056 Aachen, Germany

(Received 15 December 1998)

The magnetism, structure, and growth of thin Mn films on $Cu_3Au(100)$ have been investigated by low-energy electron diffraction (LEED) including I/V measurements, Auger electron spectroscopy, medium-energy electron diffraction, and the magneto-optical Kerr effect. Up to 20 ML Mn could be grown layer by layer. The films adopt the in-plane spacing of the $Cu_3Au(100)$ substrate. The LEED $I(V)$ analysis finds two different structural phases. Their atomic volume differs by 7%. In addition, both structures have different tetragonal distortions. The interior of thick Mn films is characterized by a considerable tetragonality of a cubic phase. Such a distortion is also found for Mn on Ag(100) [P. Schieffer, C. Krembel, M. C. Hanf, D. Bolmont, and G. Gewinner, J. Magn. Magn. Mater. **165**, 180 (1997)], even though the atomic volume of these films is larger by 10%. Both structures can be attributed to elastic deformations of a single phase. The absence of any measurable Kerr ellipticity as well as the tetragonal distortion of this structure can be explained by a particular arrangement of magnetic moments in an antiferromagnetic phase. [S0163-1829(99)02832-5]

I. INTRODUCTION

Bulk manganese has one of the richest varieties of crystallographic and magnetic phases known for metallic elements. As a function of temperature, four different modifications are observed. In bulk Mn, the complex α phase is stable up to approximately 1000 K. This phase has 58 atoms in the unit cell, an is characterized by hexatetrahedral building blocks with nearest-neighbor spacings that vary between 2.24 and 3.0 Å. The complex cubic β phase with 20 atoms per unit cell is stable between 1000 and 1368 K. The γ and δ modifications are face-centered-cubic and body-centered-cubic, with a nearest-neighbor spacing of 2.73 Å at 1373 K and 2.67 Å at 1413 K, respectively. γ-Mn is stable between 1368 and 1406 K, while δ-Mn is stable between 1406 and 1517 K. While α-Mn is antiferromagnetic below 100 K, the other phases are paramagnetic at the temperatures at which they exist.

Therefore, this material has also attracted considerable theoretical interest.[2–5] Particular emphasis was put on the simpler γ and δ phases of Mn. Oguchi and Freeman[5] were the first to point out why γ-Mn should be tetragonally distorted when it is antiferromagnetically ordered. Indeed, their calculation could reproduce the tetragonal distortion of Mn-rich bulk alloys at low temperature. Recently, several first-principles calculations have also been performed. For example, total-energy calculations by Asada using the spin-density approximation with the generalized gradient approximation have addressed the question of the magnetic ground state of fcc and bcc Mn.[2] These computations predict a ferromagnetic ground state for bcc Mn and an antiferromagnetic ground state for fcc Mn. Until now the results of these calculations have been mostly compared with data for bulk alloys. Even though lattice parameters for such systems can be determined with high precision, additional elements have to be added to Mn to stabilize the γ phase. Therefore, it is not surprising that a considerable variation in lattice parameters and tetragonal distortions has been found. The atomic volume varies between 11.82 and 12.97 $Å^3$ (Refs. 6–8) and the c/a ratio between 1.34 and 1.39.[6–8]

In recent years an interesting approach has been pursued to determine the structural properties of metastable phases. Epitaxial growth enables the stabilization of structural phases. The interatomic spacing of the Mn-rich alloys is between 2.60 and 2.68 Å, and so very close to the interatomic spacing of 2.65 Å in Cu_3Au. As a consequence, epitaxial growth of Mn on $Cu_3Au(100)$ might enable the stabilization of antiferromagnetic Mn in the tetragonally distorted fcc phase. This phase is particularly interesting, since not all of the magnetic moments can couple antiferromagnetically. Spins of four nearest neighbors are aligned parallel in the (100) plane: Spins in the fcc lattice are therefore frustrated. This is schematically depicted in Fig. 1(a). As a consequence the magnetic moments in the fcc lattice do not have to be collinear. The fcc lattice can be subdivided into sublattices containing spins which compensate for each other. The three different possible spin orientations are displayed in Fig. 1(b) to Fig. 1(d). The simple spin-density wave (SSDW) describes the collinear case, in which the magnetization vector **m** lies in the [001] direction [Fig. 1(b)]. The double-spin-density wave (DSDW) is characterized by a magnetization in the [011] and [011] directions [Fig. 1(c)]. For the triple-spin-density wave, finally, the **m** vectors point in all three space directions [Fig. 1(d)]. Crockford calculated the total energy

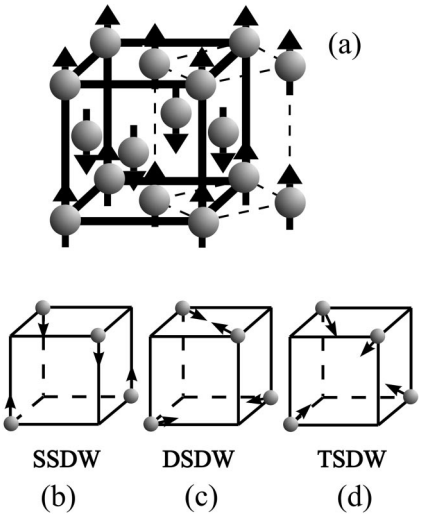

FIG. 1. Antiferromagnetic spin structure in a fcc crystal [Fig. 1(a)]. Four of the 12 moments of nearest neighbors are aligned parallel, the remaining eight are aligned antiparallel. In such a frustrated spin lattice the moments do not need to be aligned collinear. (b)–(d) show the possible antiferromagnetic spin structures of a fcc lattice. The simple spin-density wave (SSDW) in (b) is characterized by a collinear alignment of moments in the [100] direction. Only a sublattice is shown for clarity. In the DSDW, the moments are aligned in the [011] and [011] directions (c). In the triple-spin density wave (TSDW), finally, the moments are aligned in the [111] directions (d).

for these three spin orientations.[3,4] These investigations show that the total-energy differences are rather small. But the interaction of adjacent moments for the three different spin structures is rather different.[4,5] Therefore, a change in the interatomic spacing will have different consequences depending upon the orientation of the magnetization vector. This can lead to a tetragonal distortion of the fcc lattice for antiferromagnetic Mn, where the sign and size of the distortion depend upon the magnetization vector. Recent calculations[9,10] considerably expand the studied range of magnetic couplings and geometric arrangements of the atoms (the c/a ratio and atomic volume). Nevertheless, there is still a clear correlation between the magnetic coupling and the film structure. Hence a precise determination of the structure of antiferromagnetic Mn should allow a determination of the spin structure. With this goal in mind we have studied the structure, growth, and magnetism of Mn on $Cu_3Au(100)$. In Sec. II, we give a brief description of our setup and experimental procedures. Experimental results are presented in Sec. III. A discussion and comparison with previous work both for Mn bulk alloys and epitaxial Mn films is the subject of Sec. IV.

II. EXPERIMENT

The experiments in this study were performed in an ultrahigh-vacuum chamber, which contains all facilities necessary to prepare the substrate and films as well as to analyze their structural and magnetic properties. Only a brief description of the system will be given here because the apparatus and our sample treatment have already been described elsewhere.[11] The substrate was a polished $Cu_3Au(100)$ single crystal, oriented to within 0.1° of the surface normal. The surface was cleaned by cycles of Ar sputtering and annealing until the contamination level was below the Auger detection limit. Mn was evaporated from an alumina crucible with a deposition rate between 0.1 and 0.4 ML/min. During Mn deposition the pressure did not exceed 1×10^{-8} Pa. After the source was turned off, it quickly dropped to a base pressure of 4×10^{-9} Pa. The film growth was monitored by measuring the medium-energy electron-diffraction (MEED) intensity during deposition employing an electron energy of 3 keV. Regular oscillations, which are indicative of layer-by-layer growth, allow a precise thickness determination. To investigate structural properties, a low-energy electron-diffraction (LEED) pattern was observed, and spot profiles were measured in different crystallographic directions. The intensity of several LEED beams was recorded as a function of electron energy. These LEED I/V curves were used as input for a quantitative, full-dynamical structure analysis. Furthermore, a comparison of I/V curves was used to detect changes of structural properties with film thickness. Magnetic properties of the films were characterized using the magneto-optic Kerr effect. A He-Ne laser with a wavelength of 632.8 nm was used as the light source.

TABLE I. Dependence of the onset of diffusion upon the Mn film thickness. T_{diff} is the annealing temperature of the Mn film which leads to a change of the 60-eV Cu or 69-eV Au Auger signal. This change is indicative for the onset of Cu, or Au diffusion, respectively, to the film surface.

Film thickness (ML)	Cu(T_{diff})	Au(T_{diff})
2.6	328	328
5.0	453	423
9.0	473	473
18.0	503	503

III. RESULTS

A. Growth and morphology

Mn forms ordered bulk alloys with Au and disordered bulk alloys with Cu. Hence interdiffusion between Mn and the Cu_3Au substrate must be suppressed to stabilize Mn films on $Cu_3Au(100)$. Therefore, we have initially studied the interdiffusion of Mn, Cu, and Au. Mn films were deposited at 170 K. The intensity of several Auger transitions at low energy (Mn 40 eV, Cu 61 eV, and Au 69 eV) was measured after deposition. Subsequently the temperature was raised in steps of 30 K. After 20 min at constant temperature, the Auger intensity ratios were determined again. A change of the Auger intensity ratio after such an annealing step is indicative for interdiffusion. The temperatures T_{diff}, at which an interdiffusion is observed, are listed for different film thicknesses in Table I. For small thicknesses such as 2.6 ML, the onset for interdiffusion is observed slightly above room temperature. The onset temperature for interdiffusion increases with film thickness. The interdiffusion of Au is observed for film thicknesses up to 6 ML at a fairly lower temperature than Cu, but above this thickness the difference vanishes. For film thicknesses between 9 and 18 ML, the onset temperature for interdiffusion occurs between 470 and

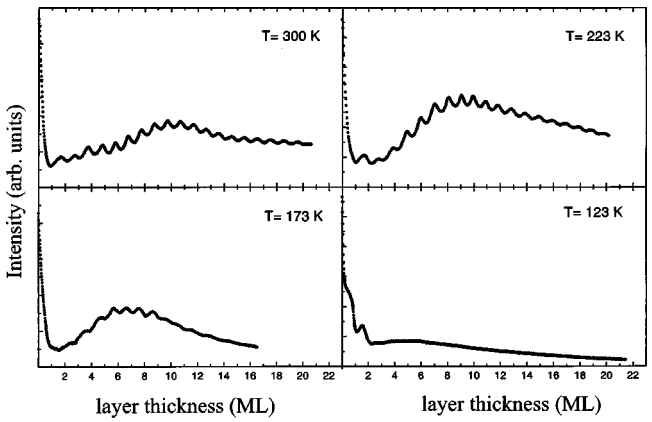

FIG. 2. MEED curve of the (0,0)-spot intensity during deposition at various growth temperatures. The curves were recorded with an electron energy of 3 keV and an angle of incidence of 81.4° against the surface normal.

500 K. This value is lower than expected for a film dominated by volume diffusion. This indicates that defects are present in the Mn film, which offer alternative diffusion pathways such as grain boundary diffusion with a lower activation energy.[12] For structural analysis, films were deposited at 173 K. They were subsequently annealed at 300 K to decrease the roughness and increase the order of the film. To study growth of Mn films in more detail, MEED curves were recorded for different deposition temperatures (Fig. 2). At 300 K, pronounced oscillations are observed which are characteristic of layer-by-layer growth. Oscillations are observed up to 20 ML at a deposition temperature of 223 K. With a further decrease in growth temperature these oscillations are less pronounced and restricted to the first 10 ML. Below 160 K, a more or less continuous decrease in intensity is observed. The disappearance of intensity oscillations and the decreasing intensity results from three-dimensional growth caused by the decreasing mobility of deposited atoms. A second characteristic feature of MEED curves recorded for

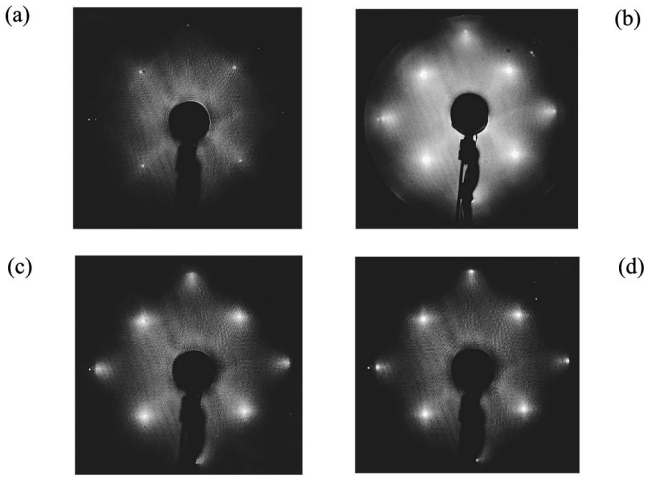

FIG. 3. LEED pattern of Mn films with increasing film thickness. Mn films were deposited at 173 K, and subsequently annealed at 300 K for 10 min. All images were recorded at 100 K. The coverage increases from 2.6 ML (a) to 6.7 ML (b) 7.9 ML (c), and 16 ML (d). The first three images were recorded with an electron energy of 112.5 eV (d) at 117.2 eV.

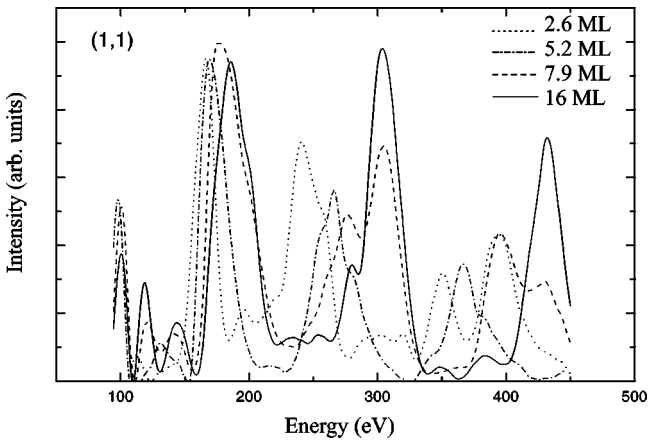

FIG. 4. LEED I/V spectra for the (1,1) beam as a function of electron energy for four different film thicknesses. All films were deposited at 173 K and annealed at 300 K. The changes of the peak positions indicate considerable structural changes of the Mn films with increasing coverage.

growth temperatures between 173 and 300 K is an increase of the average intensity upon increasing film thickness. Mn deposition at 173 K, for example, leads to a broad intensity maximum around 7 ML and a clear minimum around 1.5 ML. Similar changes are also visible in Fig. 2 for growth temperatures of 223 and 300 K. It is interesting to note, that the oscillation amplitude is largest for those film thicknesses where the average intensity is highest. To comprehend this observation fully, it is necessary to determine the structure of the Mn films with growing thickness.

B. Structure

Figure 3 shows the LEED pattern of Mn films with increasing coverage. Independent of film thickness, no superstructure beams were induced by the deposition of Mn atoms. For a 2.6-ML thick Mn film, in addition to the sharp substrate beams, a weak and diffuse spot broadening in the [011] direction is observed, which is independent of electron energy. After deposition of 6.7-ML Mn, the spot broadening runs in the [011] direction, and the background intensity is considerably increased. A further increase in film thickness leads to a decrease in the half-width of the beams and a reduced background intensity. This implies that the structural order of the Mn films deposited at 173 K is best for small thicknesses below 3 ML and large thicknesses above 12 ML. The high average intensity and large oscillation amplitude of the MEED curves coincide with the thickness region where the corresponding LEED pattern shows the highest background intensity. To obtain a first qualitative impression of the thickness-dependent structure, we measured LEED spot profiles. With this measurement we verified that the position of the LEED beams does not vary with thickness. This implies that the in-plane lattice spacing is independent of the film thickness in the studied range. For a more detailed characterization of film structure, LEED I/V curves for several beams were recorded for different film thicknesses. A comparison of spectra for the (1,1) beam is shown in Fig. 4. With increasing film thickness, pronounced peak shifts are observed. The spectra for 2.6- and 5.2-ML thick films deviate considerably from the spectrum of a 16-ML thick film. The

7.9-ML thick film, however, already resembles the thicker Mn film. This implies that the film structure changes drastically between 5 and 8 ML. It is tempting to relate changes in peak position directly to a change of interlayer distances. However, a precise structure determination is only possible with a full dynamical analysis of the data.

For small thicknesses a precise film structure determination is considerably more complex than for thicker films. For thin films the structure of the substrate surface and a possible interdiffusion at the interface need to be included. Therefore we have started to analyze the LEED I/V data of thicker Mn films. For the 16-ML thick Mn film the precise atomic arrangement of the substrate surface is irrelevant,[13] and interdiffusion at the interface can be neglected as well. Since the LEED data show compelling evidence of a structural change of the Mn films around 6 ML, we have also tried to determine the structure of the 5.2-ML thick film, neglecting the precise atomic arrangement at the interface. This approach can be justified since the measured I/V curve is dominated by the contribution of the first 4–5 layers.

LEED I/V curves were measured at 140 K for a film deposited at 173 K, and subsequently annealed for 10 min at 300 K. The incident beam was adjusted close to normal incidence, about 1.5° in the [011] direction and the energy was varied in the range of 50–500 eV. Calculations were performed up to 450 eV with a cumulated energy range of 2495 eV for nine inequivalent beams for the 16-ML thick film and of 1430 eV for six inequivalent beams for the 5.2-ML thick film.

1. Calculations

For the full dynamical calculations, we used the same standard FORTRAN code[14] and phase shifts as in our previous studies of thin Mn films and Cu-Mn surface alloys.[15–17,20] The Debye temperature was originally assigned a value of 440 K, and was let free to vary in some runs for the two surface layers of the 16-ML thick film and for three surface layers of the 5.2-ML thick film. However, as the Mn film grows with a lattice constant and structure which differs from that of bulk Mn, we also checked the bulk Debye temperature. Both fixed and energy-dependent refraction (V_0) and absorption (V_i) potentials were tested. For the thicker Mn film, lower r factors were reached using $V_i = 6.5$ eV and $V_0 = -12$ eV, a rigid shift being allowed in each run. For the thin film we found energy-dependent potentials to fit best. The best r factors were obtained by using $V_i = 9.0$ eV and $V_0 = -1.7E^{1/3}$, where E is the electron energy in eV. The optimum model search was conducted with different r-factors[18] and metric distances.[19,20] Error bars are derived from the variance of the numerical criteria as defined by Pendry:

$$Var(R_p) = R_{p,\min}\sqrt{8V_i/\Delta E}, \tag{1}$$

$$Var(R_{DE}) = R_{DE,\min}\sqrt{2.4V_i/\Delta E}, \tag{2}$$

with ΔE the energy range where theory and experiment overlap. Owing to the relatively large film thickness of 16 ML (≈ 30 Å), which is close to the convergence limit in LEED calculations, it was assumed that the influence of the substrate is negligible. In the program package used we varied the first three Mn layers spacings and the bulk layer distance of the Mn film. The same strategy was also adopted for the 5.2-ML thick Mn film. Employing a semi-infinite Mn film in the calculations is a much cruder assumption here. Nevertheless the measured intensity should be mainly determined by the first few layers. Tests were also made with a Cu_3Au substrate, which led to structural parameters very similar to the ones presented in Sec. III B 2. This renders additional support to our approach. Furthermore, in the calculation, the Debye temperature and to some extent the absorptive and inner potential were varied as well. In addition the interatomic distance in the (100) plane was determined, even though LEED spot positions did not change upon Mn deposition, which implies that the Mn atoms adopt the interatomic distance of 2.652 Å of the Cu_3Au surface.

TABLE II. Optimum parameters for R_p for the 5.2- and 16-ML-thick Mn films. d_{ij} is the interlayer distance between layer i and j, Θ_{Di} is the Debye temperature of layer i, and a_p is the in-plane nearest-neighbor spacing. The index b denotes the bulk parameter, while ΔE is the energy overlap between calculated and experimental $I(V)$ curves.

Parameter	5.2 ML	16 ML
R_p	0.215	0.156
d_{12} (Å)	1.93±0.025	1.88±0.023
d_{23} (Å)	1.91±0.025	1.775±0.015
d_{34} (Å)	1.92±0.08	1.78
d_b(Å)	1.99±0.12	1.772
a_p(Å)	2.67±0.06	2.642±0.015
Θ_{D1} (K)	150	215
Θ_{D2} (K)	370	405
Θ_{Db} (K)	440	490
ΔE(eV]	1430	2495

2. Results

Calculations started with the analysis of the thicker Mn film. The first runs were devoted to determining the angle of incidence simultaneously with a rough estimate of the bulk interlayer spacing. Only two parameters—the interlayer distances d_{12} and d_{23}—were allowed to vary in each run. Once the vertical spacing was located around 1.80 Å, we varied the angle of incidence in steps of 0.5°. The optimum was found at 1°, but a later refinement, when a much better agreement was obtained by letting free all other parameters, led to the final value of 1.4°. Quite soon, we controlled the lateral lattice constant because a wrong figure would distort the other geometrical parameters. Within the precision of the technique, in this preliminary step, we conclude that the Mn film grows with exactly the Cu_3Au constant, that is in perfect epitaxy with the substrate. Also for this parameter, a final check, performed after optimization of the other parameters, confirmed the original finding: R_{de} and R_p have minima at 2.662 and 2.642 Å with a mean value of $a = 2.652$ Å, which is exactly the alloy substrate parameter in Table II. This is in line with the observation that the LEED spot position does not change upon increasing Mn film thickness. The Debye temperature in the bulk happens to differ slightly depending on the criteria used to assess the quality of the fit.

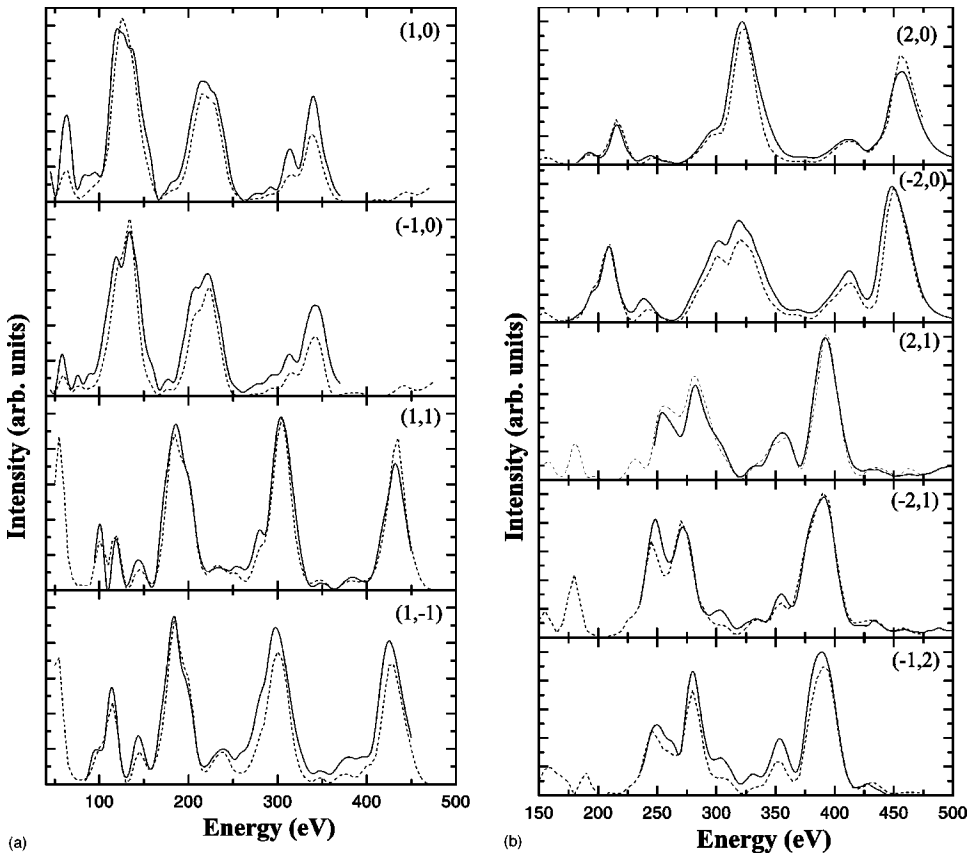

FIG. 5. Comparison of calculated (dashed line) and measured (solid line) I/V spectra for a 16-ML thick Mn film. Both the peak positions and the absolute intensities are reproduced very well by the calculations using the structural parameters listed in Table II.

The bulk value ranges from 490 to 610 with a mean value of 550 K, which was kept for the rest of the analysis. In the surface layers, the situation is quite different: the second layer has an optimum around 400 and 480 K for R_p and R_{de}, respectively, while the top layer ends with a quite low value of about 200 K (Table I). In the final step—refinement of the d_{12} and d_{23}, surface compositions with fixed bulk parameters and incidence angle—the r factors decrease to rather low figures, $R_p = 0.156$ ($\Delta R_p = 0.023$) and $R_{de} = 0.210$, implying a very good agreement between experimental and theoretical spectra. This is nicely confirmed by visual inspection of the spectra of Fig. 5 presented for near-optimum parameters. Every feature of the experimental curves is perfectly reproduced by the calculation, even the smallest ones. Similarly, the peak positions do coincide ideally while the width, but for one or two peaks they fit quite well. This would not occur if one of the lattice distances or the absorption potential would be wrong. The only weak discrepancies are related to the relative height of peaks which may derive from imperfections in either the LEED screen, such as small inhomogeneities, or in the data acquisition, such as background subtraction, for example. This is visible for the three low-index beams and more particularly in the range from 100 to 200 eV, where some intensity is missing in the highest peaks. In this energy range, the low-index beams are closest to the edge of the screen, and hence particularly prone to experimental difficulties in the precise intensity determination. The most important outcome of the structure analysis is the layer stacking and the relative position of the layer. Whereas the lateral spacing is that of the Cu_3Au substrate (2.65 Å), a clear and single minimum is found at 1.772 Å for the interlayer spacing of the bulk layers of Mn. This is much smaller than the fcc spacing of the substrate of 1.875 Å. The same distance 1.77 Å is found, within 0.01 Å for the second and third interlayer distances (Fig. 6). Hence the resulting structure is a tetragonally distorted fcc structure. In comparison, the top layer spacing, d_{12}, is noticeably larger, with a figure of 1.873 Å, which is close to that of Cu_3Au. This is a 6% expansion with respect to the Mn bulk.

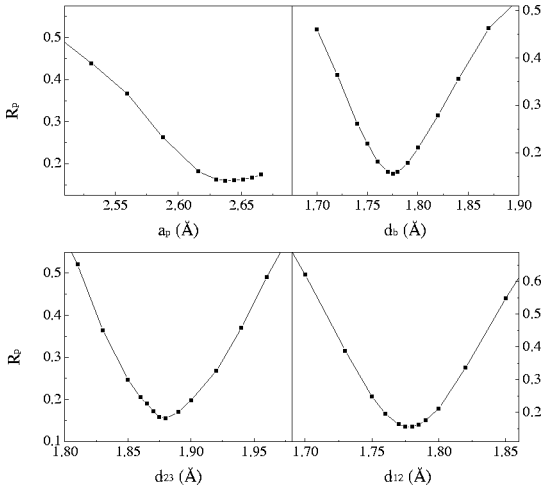

FIG. 6. Variation of the Pendry R factor vs the in-plane lattice constant, and the first surface and bulk interlayer distances for the 16-ML thick film.

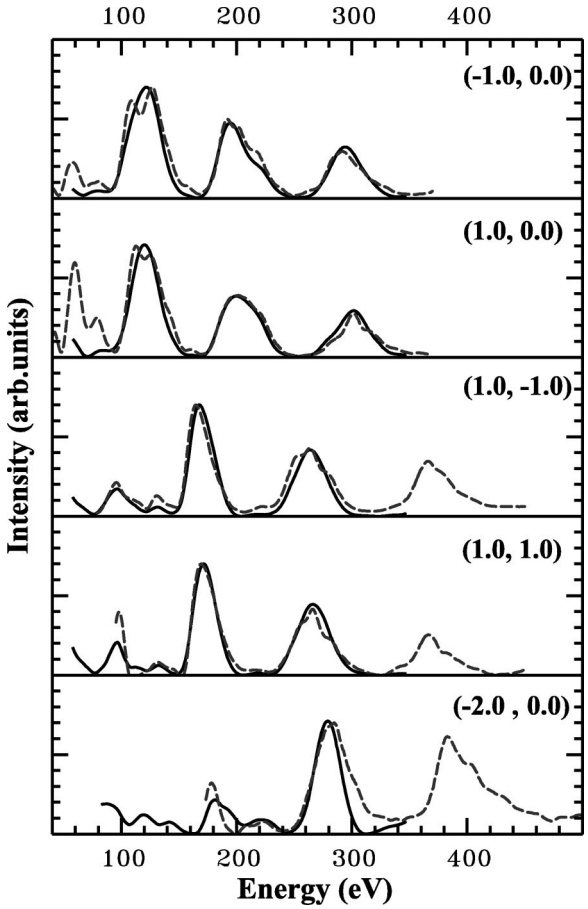

FIG. 7. The dashed curves denote the experimental $I(V)$ curves and the solid curves the best fit structure calculated for the 5.2-ML-thick Mn film.

Such an expansion is quite unusual at the unreconstructed (100) surfaces of fcc crystals. For metals as well as alloys the corresponding spacing is usually equal to the bulk interlayer spacing within 1–2 %.

The structure determination for the 5.2-ML film was performed similarly to that for the structure analysis of the thick film ($R_p = 0.215 \Delta R_p = 0.048$). For the in-plane lattice spacing a parameter of 2.67 ± 0.04 Å was determined, which agrees well with the atomic distance of Cu and Au atoms in the (100) substrate planes. This result again corresponds to the analysis of the LEED beam positions. The R factor is roughly 50% higher for the 5.2-ML thin Mn film compared to the thick film. Nevertheless, a visual inspection of Fig. 7 shows that for most peaks the position is fairly well reproduced by the calculations. The main discrepancy is in the relative intensity of some peaks. This implies that we correctly describe the major features of the film structure. The resulting parameters for the interlayer spacing are shown in Table II. Interestingly enough, the interlayer spacing between the third and fourth layers and the bulk value deviate strongly from the values for the thick Mn films. For the 5.2-ML film, a value of 1.92 Å is found for d_{34}. The resulting c/a ratio of 1.437 closely resembles an almost cubic structure ($c/a = 1.414$), which is in striking contrast to the tetragonal distortion observed for the thicker Mn films ($c/a = 1.347$).

The first two layers also show a large interlayer spacing of 1.925 and 1.91 Å respectively. Hence, we have a considerable expansion at the film surface for 5.2- and 16-ML thick films, but a distinctly different interlayer spacing in deeper layers, even though the in-plane spacing is the same within 1%. In the discussion we will come back to this remarkable observation. Finally we also checked for the composition of the film surface and the bulk layer of the 16-ML film. The different layers were assumed to be a random mixture of different species (Cu, Au, and Mn) and were then treated with the ATA approximation.[21] For technical reasons, the program can handle only two species for one layer and the Cu and Au concentration were optimized versus the Mn fraction separately. Considering a Mn-Au mixture, the optimum clearly occurs for a pure Mn layer. Conversely, the presence of 10–15 % Cu results in a slight improvement of both r factors. Mn and Cu are quite close in the Periodic Table, and hence only show weak differences in the phase shifts. Therefore the curvature is not very pronounced and the conclusion is not really clearcut. Nevertheless, the presence of a few percent Cu, not fully consistent with the Auger electron spectroscopy results, cannot be excluded. Meanwhile, these foreign atoms do not modify the answer with respect to the geometrical parameters. Similar conclusions were also derived for the 5.2-ML film.

C. Magnetism

To determine the magnetic ground state of the manganese films, the magneto-optic Kerr effect (MOKE) was employed. Mn films with thicknesses up to 25 ML were investigated using MOKE by applying both a modulation technique[12] and null-ellipsometry[22] at sample temperatures between 100 and 500 K. No evidence of a ferromagnetic coupling was found. We have also tried to find proof for an antiferromagnetic coupling in the Mn films. In a study of Fe film wedges on Cu(100) Li *et al.*[23] found evidence of an antiferromagnetic coupling of adjacent iron layers from an oscillation of the Kerr signal with film thickness. We have carefully looked for evidence of such an antiferromagnetic coupling of the Mn layers using MOKE, but could not find any. Hence only a ferromagnetic coupling of the Mn films with a Curie temperature above 100 K can be unequivocally excluded.

IV. DISCUSSION

Both thick and thin Mn films grow pseudomorphically on the $Cu_3Au(100)$ substrate. The most prominent finding of our LEED analysis is a considerable tetragonal distortion for bulk-like layers and an expansion of the interlayer spacing at the film surface. While the latter observation holds for both film thicknesses (5.2 and 16 ML), the tetragonal distortion differs considerably for these films. The structural transition occurs at a critical thickness between 5.2 and 8 ML as indicated by the marked changes in the $I(V)$ spectra (Fig. 4).

We are now facing the task of deriving the unstrained ground state of Mn from the results of our structure determination. To achieve this goal, two different procedures are possible. In principle, the precise knowledge of both elastic constants and the equilibrium structure of a body centered tetragonal Mn *bulk* phase would enable the prediction of the tetragonality of Mn on $Cu_3Au(100)$ within the framework of

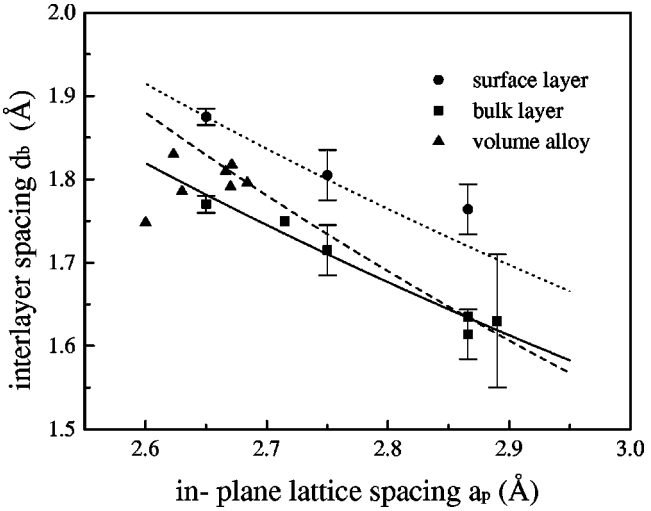

FIG. 8. Interlayer spacing as a function of the in-plane spacing for different Mn structures. The squares show the data points for bulk layers determined by previous studies [Mn on Ir (Ref. 24), on Fe (Refs. 25 and 26), on Ag (Refs. 1 and 27), and on Pd (Ref. 28)] and in this work for the 16-ML thick film on $Cu_3Au(100)$. The straight line is the fit for the interlayer spacing as a function of the in-plane spacing using Eq. (3). The triangles show data for Mn bulk alloys (Refs. 6–8) and the circles the available data for the surface interlayer spacing [Mn on Fe (Ref. 25) and on Pd (Ref. 28)]. The dashed line shows the fit for the data points of the bulk layers with the assumption that the data point of Endoh and Ishikawa desribes the equilibrium structure. The dotted line is a guide to the eye.

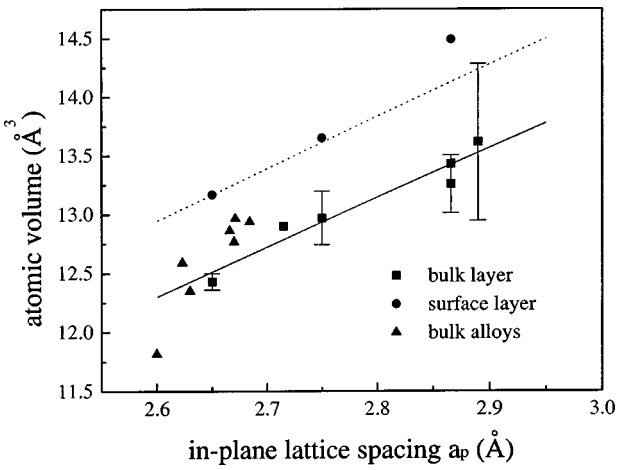

FIG. 9. The figure shows the dependence of the volume on the in-plane lattice parameter. The squares show the bulk volume [Mn on $Cu_3Au(100)$ this study, Mn on Ir (Ref. 24), on Fe (Refs. 25 and 26), on Ag (Refs. 1 and 27), and on Pd (Ref. 28)] the circles the surface volumes [Mn on Fe (Ref. 25 and on Pd (Ref. 28)] and the triangles the values for different Mn bulk alloys (Refs. 6–8). The straight and dotted lines are based on the fit in Fig. 8.

elasticity theory. Unfortunately, the structure determination for this phase shows considerable scatter in atomic volume and c/a ratio, and no data are available for elastic properties. Hence we will initially adopt a different procedure. Nevertheless, we will come back to this approach at the end of this section. At first, however, we try to identify generic aspects in previous experimental studies of the structure of Mn *films*. We will focus on substrates with a lattice spacing similar to the one of $Cu_3Au(100)$. The studies include Mn on Ir(100) (Ref. 24) (using extended x-ray-absorption time structure), on Fe(100) [using LEED $I(V)$ (Ref. 25) and kinematical LEED (Ref. 26)], on Ag(100) (Refs. 1 and 27) (using x-ray diffraction and XPD), and on Pd(100) (Ref. 28) [using LEED $I(V)$].

These studies show a number of trends similar to our findings. In particular an interlayer expansion at the film surface is frequently observed.[25,28] In addition, compelling evidence for two different structures with increasing thickness is found for several systems.[25,1,28] Finally, all studies observe that Mn grows pseudomorphically on the different substrates. This is indicative of a complex interaction between structure, elastic, electronic, and possibly also magnetic properties. To obtain a more quantitative description of the various film structures, we have plotted the bulk interlayer distance d versus the in-plane nearest neighbor distance (a_p) for all studies (Fig. 8). d_b is the half unit-cell parameter c. According to elasticity theory,[29,30]

$$c = c_{\mathrm{eq}}\left(\frac{a}{a_{\mathrm{eq}}}\right)^{-\gamma} \tag{3}$$

where eq describes equilibrium values and γ is $2\nu/(1-\nu)$ with ν the Poisson ratio. We have tried to fit the experimental data with one single fit by assuming a value for a_{eq}, and fitting for c_{eq} and γ. A similar approach was recently pursued by Kim *et al.*[25] Indeed Fig. 8 shows that with $a_{\mathrm{eq}} = 2.65$ Å, a good fit is obtained for $c_{\mathrm{eq}} = 3.56 \pm 0.03$ Å and $\gamma = 1.10 \pm 0.11$. This describes the data for a rather wide range of in-plane lattice spacings. Clearly our choice of a_{eq} influences c_{eq}, but the value of γ is independent of the choice of a_{eq}. From $\gamma = 1.10 \pm 0.11$, ν can be determined to 0.35 ± 0.03. This value is slightly lower than the value found for γ-Ni ($\nu = 0.38$) or γ-Co ($\nu = 0.40$).[31] However, our finding is in contrast to the work of Kim *et al.*,[25] who reported a value of 0.45–0.50 for ν. This would correspond to a rather soft phase, while our finding implies a considerable hardness of tetragonal Mn. Furthermore, the available data[6–8] for different Mn bulk alloys are displayed for comparison in Fig. 8.

In addition, we have also plotted the interlayer spacing in the vicinity of the surface against the in-plane spacing for the existing data. Since only three data points are available, no conclusive determination of γ is possible. However, it seems as if the elastic behavior can be reproduced sufficiently well with a γ of 1.10. The same value was also used to fit the bulk data.

In Fig. 9, the atomic volume has been plotted versus the in-plane nearest-neighbor spacing. In this diagram we have also included data points obtained by comparison with data of the structure of Mn-rich alloys,[6–8] where the structure was extrapolated to pure Mn (triangles). This leads to atomic volumes around 12.5 Å^3 and an in-plane spacing around 2.65 Å. These data closely resemble the structure we find for Mn on $Cu_3Au(100)$ with $a_p = 2.65$ Å and an atomic volume of 12.4 Å^3. The compilation of data for Mn films on other substrates shows that the volume increases nearly linear with increasing a_p for both bulk and surface layers. For the bulk layer, the volume increases to 13.6 Å^3 for $a_p = 2.89$ Å. This corresponds to a remarkably large 10% in-

crease in atomic volume. Such an expansion is considerably larger than the 6% volume expansion from the AFM fcc iron phase to the FM fcc iron modification found in thin Fe films on Cu(100).[32,33] This raises the question if the different atomic volumes of Mn are related to different magnetic states. Interestingly enough, several theoretical studies investigated the magnetic ground state of tetragonal bulk Mn as a function of the volume and the c/a ratio, and found different magnetic phases for different structures.[9,10] In all studies an antiferromagnetic phase over a wide range of atomic volumes and c/a ratios is favored. This is in line with the experiments. To our knowledge, no experimental evidence for *thicker* Mn films with ferromagnetic coupling has been reported as yet. For thick films on $Cu_3Au(100)$, we do not observe any Kerr rotation over a wide range of thicknesses and substrate temperatures. Such an observation could be explained by an antiferromagnetic phase.[34–37] Theoretically a large number of different antiferromagnetic structures has been studied. These phases are stabilized for different c/a ratios. As shown in Refs. 2, 38, and 3, a c/a ratio smaller than $\sqrt{2}$ can be attributed to a SSDW [see Fig. 1(a)]. This would imply that Mn films on Cu_3Au have this structure. Recent calculations[9,10] consider additional models for AFM coupling, and explore a wide range of parameters. They show that for a c/a ratio between 1.2 and 1.4, two different couplings could be stabilized.[9] For the atomic volume we find, however, one would expect an AF1 (SSDW) structure. This implies that the structural and magnetic data we observe for thick Mn films are consistent with an antiferromagnetic SSDW.

The situation is less clear for the surface interlayer spacing of thin Mn films. We observe an increased average atomic volume of 13.3 $Å^3$. This is approximately 7% larger than the atomic volume of thick Mn films. A similar scenario has also been reported for Fe on Cu(100),[32,33] where the change in atomic volume is correlated with a change in magnetic coupling from ferromagnetic to antiferromagnetic. For Mn on $Cu_3Au(100)$ no evidence for a ferromagnetic coupling is observed. On Ag(100), a similar increase of atomic volume is found in the surface vicinity of thin Mn films. Nevertheless, one other study finds a rather different structural behavior. For Mn on Fe(100), a decreased interlayer spacing is observed for 1 ML. Possibly such a finding can be attributed to the magnetic coupling to the underlying substrate. Further studies are clearly necessary to confirm unique trends for thin Mn films.

As mentioned in the beginning of this section a different approach would have been to compare our data with structural parameters derived from the study of Mn-rich bulk alloys. This approach is graphically visualized in Fig. 8 as well. We have chosen the structure determination of Endoh and Ishikawa[7] as a reference point. Fitting the thin-film data with this reference leads to the dashed line in Fig. 8. The fit leads to a slightly worse overall agreement, and produces a rather different value for ν of 0.42. This would imply that Mn is rather soft in a reasonable agreement with the analysis by Kim *et al.*,[25] which concludes that ν is equal to 0.45 to 0.5. A determination of the elastic properties of Mn films should allow the determination of ν, and hence enable one to decide which fit is correctly describing the structural behavior of the films. We have to add, however, that even with an experimental value of 0.35 for ν we are still running into a problem with the reference point for the description of our film structure. This is already visible in Fig. 8, which shows that both a and c for the Mn films on $Cu_3Au(100)$ are smaller than the reference structure.[7] Such a behavior is inconsistent with elasticity theory. At present, we cannot offer a convincing solution for this dilemma. As mentioned above, a determination of elastic properties would at least show which of the two competing descriptions is correct.

V. SUMMARY

We have presented a complete LEED $I(V)$ analysis for a 5.2- and 16-ML thick Mn film on Cu_3Au. These two film thicknesses represent different structural phases. Our analysis shows that both film structures differ considerably in atomic volume and c/a ratio. Nevertheless, both films grow with the in-plane spacing of the substrate. In addition, they are characterized by an enlarged interlayer spacing at the surface. Interestingly enough, similar trends have also been observed for other Mn films. At present there is no explanation for the structural phase transition at relatively high film thicknesses. Since both phases have the same in-plane spacing, we can exclude that the reduction of misfit strains is the driving force for the transition. Further studies of the electronic and magnetic properties of the Mn films might identify the driving force for the phase transition. The tetragonal distortion and the absence of any Kerr rotation in the thick Mn films can be explained by an antiferromagnetic SSDW. A direct observation of the magnetic order could verify this interpretation. We have compared our structural results with previous studies. A considerable range of data points can be fitted by elasticity theory. From this fit the Poisson ratio of Mn is determined to 0.35 ± 0.03. This implies that Mn films are rather hard. This conclusion is in contrast to a recent analysis which concludes that Mn films are rather soft. The determination of elastic properties could settle this issue. For thin Mn films, a second state is observed, in agreement with several previous studies of Mn films on various substrates. However, a precise identification of this phase is impossible due to the considerable scatter of structural data on different substrates.

ACKNOWLEDGMENTS

We gratefully acknowledge financial support by the Deutsche Forschungsgemeinschaft (Grant No. Wu 243/2). Furthermore, we are grateful to the Institut du Développement et des Resources en Informatique Scientifique for support with computing time. The authors are indebted to W. Moritz for providing his code for the calculation of LEED intensities.

[1] P. Schieffer, C. Krebel, M. C. Hanf, D. Bolmont, and G. Gewinner, J. Magn. Magn. Mater. **165**, 180 (1997).
[2] T. Asada and K. Terakura, Phys. Rev. B **47**, 15 992 (1993).
[3] D. J. Crockford, D. M. Bird, and M. W. Long, J. Phys.: Condens. Matter **3**, 8665 (1991).
[4] D. J. Crockford, D. M. Bird, and M. W. Long, J. Phys.: Condens. Matter **4**, 2079 (1992).
[5] T. Oguchi and A. J. Freeman, J. Magn. Magn. Mater. **46**, L1 (1984).
[6] W. B. Pearson, *A Handbook of Lattice Spacings and Structures of Metals and Alloys*, International Series of Monographs in Metal Physics and Physical Metallurgy (Pergamon, Oxford, 1967).
[7] Y. Endoh and Y. Ishikawa, J. Phys. Soc. Jpn. **30**, 1614 (1971).
[8] U. Zwicker, Z. Metallkd. **42**, 246 (1951).
[9] P. Krüger, O. Elmouhssine, C. Demangeat, and J. C. Parlebas, Phys. Rev. B **54**, 6393 (1996).
[10] V. L. Sliwko, P. Blaha, P. Mohn, and K. Schwarz, Int. J. Mod. Phys. B **7**, 614 (1993).
[11] B. Feldmann, B. Schirmer, A. Sokoll, and M. Wuttig, Phys. Rev. B **57**, 1014 (1998).
[12] J. Thomassen, Ph.D. thesis, RWTH Aachen, 1993.
[13] P. Schmailzl, K. Schmidt, P. Bayer, R. Doll, and K. Heinz, Surf. Sci. **312**, 73 (1994).
[14] W. Moritz, J. Phys. C **17**, 353 (1984).
[15] M. Wuttig, C. C. Knight, T. Flores, and Y. Gauthier, Surf. Sci. **292**, 189 (1993).
[16] M. Wuttig, Y. Gauthier, and S. Blügel, Phys. Rev. Lett. **70**, 3619 (1993).
[17] Y. Gauthier, M. Poensgen, and M. Wuttig, Surf. Sci. **303**, 35 (1993).
[18] J. B. Pendry, J. Phys. C **13**, 937 (1980).
[19] J. Philip and J. Rundgren, in *Determination of Surface Structure by LEED*, edited by P. M. Marcus and F. Jona (Plenum, New York, 1984).
[20] Y. Gauthier, R. Baudoing, Y. Joly, C. Gaubert, and J. Rundgren, J. Phys. C **17**, 4547 (1984).
[21] B. L. Gyorffy and G. M. Stocks, in *Electrons in Disordered Metallic Surfaces*, edited by P. Phariseau, B. L. Gyorffy, and L. Scheire (Plenum, New York, 1979).
[22] A. Berger, S. Knappmann, and H. P. Oepen, J. Appl. Phys. **75**, 5598 (1994).
[23] D. Li, M. Freitag, J. Pearson, Z. Q. Qiu, and S. D. Bader, Phys. Rev. Lett. **72**, 3112 (1994).
[24] S. Andrieu, H. Fischer, A. Traverse, and M. Piecuch, Phys. Rev. B **54**, 2822 (1996).
[25] S. K. Kim, Y. Tian, M. Montesano, F. Jona, and P. M. Marcus, Phys. Rev. B **54**, 5081 (1996).
[26] S. T. Purcell, M. T. Johnson, N. W. E. McGee, R. Coehoorn, and W. Hoving, Phys. Rev. B **45**, 13 064 (1992).
[27] Y. U. Idzerda, B. T. Jonker, W. T. Elam, and G. A. Prinz, J. Appl. Phys. **67**, 5385 (1990).
[28] D. Tian, S. C. Wu, and F. Jona, Solid State Commun. **70**, 199 (1989).
[29] P. M. Marcus and F. Jona, Surf. Rev. Lett. **1**, 15 (1994).
[30] F. Jona and P. M. Marcus, Surf. Rev. Lett. **3**, 1285 (1996).
[31] P. Eckerlin and H. Kandler, in *Structure Data of Elements and Intermetallic Phases*, edited by K.-H. Hellwege and O. Madelung, Landolt-Börnstein, New Series, Group III, Vol. 6 (Springer-Verlag, Berlin, 1989), Chap. 1.1.2, p. 1.
[32] J. Thomassen, F. May, B. Feldmann, M. Wuttig, and H. Ibach, Phys. Rev. Lett. **69**, 3831 (1992).
[33] S. Müller, P. Bayer, C. Reischl, K. Heinz, B. Feldmann, H. Zillgen, and M. Wuttig, Phys. Rev. Lett. **74**, 765 (1995).
[34] P. Schieffer, C. Krembel, M. C. Hanf, and G. Gewinner, Phys. Rev. B **57**, 1141 (1998).
[35] T. G. Walker and H. Hopster, Phys. Rev. B **48**, 3563 (1993).
[36] S. Andrieu, M. Finazzi, Ph. Bauer, H. Fischer, P. Lefevre, A. Traverse, K. Hricovini, G. Krill, and M. Piecuch, Phys. Rev. B **57**, 1985 (1998).
[37] Ruqian Wu and A. J. Freeman, Phys. Rev. B **51**, 17 131 (1995).
[38] M. Acet, H. Zahres, W. Stamm, E. F. Wassermann, and W. Pepperhoff, Physica B **61**, 67 (1989).